Vol. 69: 107–116, 2016
doi: 10.3354/cr01394

CLIMATE RESEARCH
Clim Res

Published online June 27

Spatial variability of daytime CO_2 concentration with landscape structure across urbanization gradients, Shanghai, China

Chen Pan[1,2], Xiyang Zhu[1], Ning Wei[1], Xudong Zhu[3,4], Qiannan She[1], Wenxiao Jia[1], Min Liu[1,*], Weining Xiang[1]

[1]Shanghai Key Laboratory for Urban Ecological Processes and Eco-Restoration, School of Ecological and Environmental Sciences, East China Normal University, Shanghai 200241, PR China

[2]School of Geography Sciences, East China Normal University, Shanghai 200241, PR China

[3]Key Laboratory of the Coastal and Wetland Ecosystems, Ministry of Education, College of the Environment and Ecology, Xiamen University, Xiamen, Fujian 361102, PR China

[4]State Key Laboratory of Remote Sensing Science, Institute of Remote Sensing and Digital Earth, Chinese Academy of Sciences, Beijing 100094, PR China

ABSTRACT: Cities play an important role in the global carbon cycle. However, direct measurements of CO_2 concentration in urban environments are still very limited. Using Shanghai as a case study, this paper investigated the spatial pattern of atmospheric CO_2 concentration and its relationship with landscape structure across urbanization gradients. From March to April 2014, CO_2 concentrations were measured at 2 m above ground level with a near-infrared gas analyzer along 6 transects with a total length of 335 km. The results showed that the mean near-surface CO_2 concentration among the 6 transects was 445.8 ± 40.5 ppm. The average CO_2 concentration in the inner city was higher (55.1 ppm) than that in the suburban area. Also, CO_2 concentration showed a significant spatial heterogeneity, with the highest CO_2 concentration in the northwest and the lowest in the southeast, in accordance with the urbanization gradients. Further analysis indicated that the spatial variability of CO_2 concentration was mainly influenced by the urban landscape structure and depended largely on the percent of impervious surface cover (ISA) with a positive correlation and on the lower explanatory power for the percent of vegetation cover (Veg) with a negative correlation. This indicated that the trend in atmospheric CO_2 in urban areas was likely to depend more on fossil fuel emissions than on vegetation change. The study also found that the Pearson's correlation (R) between CO_2 concentration and ISA or Veg achieved its highest value when the buffer distance was 5 km, which could be described by the stepwise regression equation $CO_2 = 0.99ISA - 0.18Veg + 378.18$ ($R^2 = 0.44$, $p < 0.01$).

KEY WORDS: Urban CO_2 · Mobile measurements · Underlying landscape structure · Shanghai

1. INTRODUCTION

CO_2 is one of the most important greenhouse gases in the atmosphere (WMO 2012, Stocker et al. 2013). To keep track of anthropogenic CO_2 emissions, atmospheric CO_2 concentration has been systematically monitored for decades at many ground-based sites and networks all over the world (Keeling et al. 1976, Fang et al. 2014). Notable examples include the CO_2 observations from NOAA and WMO's Global Atmosphere Watch program. However, these observations were established in undisturbed air with minimal influences of human activities (Zhang et al. 2008, Sasakawa et al. 2013). Understanding the spatial variability of CO_2 in relation to the different biophysical components of landscape structure is still

*Corresponding author: mliu@re.ecnu.edu.cn

largely required in the forecast of future CO_2 levels and the greenhouse effect (Wu et al. 2012, Stephens et al. 2013, Liu et al. 2015).

Cities play an important role in the global carbon cycle (Le Quéré et al. 2009). It is well documented that land use change and fossil fuel combustion due to urbanization have significant effects on the global carbon cycle and climate change (Churkina 2008, Le Quéré et al. 2009, IPCC 2013). From 2002 to 2011, over 70% of fossil fuel CO_2 emissions were attributable to urban areas (Energy Information Administration 2013). Understanding and quantifying the carbon cycle in cities offers a powerful lens into urban systems and provides a compact metric of urban sustainability (Hutyra et al. 2014). However, because of the high complexity and heterogeneity of the urban environment, measuring urban atmospheric CO_2 concentrations with the aim of determining the influence of local emitters of anthropogenic CO_2 sources and CO_2 sinks is still challenging (Buns & Kuttler 2012). Extensive development of CO_2 measurements in urban environments has occurred only during the past several years (Grimmond et al. 2002, Velasco et al. 2010, Grimmond & Christen 2012). Direct measurements of CO_2 concentration in urban environments are still limited compared to natural environments.

In the past 2 decades, measurements of CO_2 concentration have mainly focused on cities in developed countries, e.g. Phoenix (Idso et al. 1998, 2001), Baltimore (George et al. 2007) and Essen (Henninger 2008, Henninger & Kuttler 2010). General conclusions are that CO_2 levels reach a peak in areas with the most intense human activities and are higher in the morning than in the afternoon (Idso et al. 1998, George et al. 2007). The variations of urban CO_2 concentration are mainly influenced by local traffic conditions, meteorological conditions and land use types (Makido et al. 2012, Ou et al. 2013). However, these studies are based on continuous observations in common-point or mobile-route measurements, which could lead to difficulties evaluating the spatial and temporal variations of CO_2 concentrations at an urban scale (Kort et al. 2012). Given the spatial heterogeneity and complexity among urban ecosystems and their significance for urban landscape management and planning, it is essential to improve our understanding of the relationship between urban CO_2 concentration and the biophysical components of landscape structure at fine spatial scales.

Therefore, the objectives of this study were to investigate the spatial heterogeneity of atmospheric ambient CO_2 concentration in urban areas and to quantify the relationship between CO_2 concentration and landscape structure across urbanization gradients. To achieve these ends, we selected Shanghai, China, with its intensive human activities and rapid urbanization, as the study region. Specifically, we focused on the spatial variation of CO_2 concentration in the urban districts of Shanghai to investigate the effect of 3 biophysical components (i.e. impervious surface, vegetation and water) on CO_2 concentration. The results from this study will improve our understanding of how atmospheric CO_2 concentration varies across urbanization gradients and among different biophysical components of landscape structure.

2. DATA AND METHODS

2.1. Study area

Shanghai (30° 40′–31° 53′ N, 120° 52′–122° 12′ E), covering a total area of approximately 6340.5 km^2, is the commercial and financial center of mainland China. Located at the heart of the Yangtze River Delta in East China, Shanghai is a transport hub with the world's busiest container port. It has a humid subtropical climate and experiences 4 distinct seasons. The city averages 4.2°C in January and 27.9°C in July, has an annual mean temperature of 17.7°C, and receives 1222.2 mm of precipitation annually (2003–2014, data from Shanghai Meteorological Bureau). Shanghai car ownership was 3.04 million in 2015, and the area has an extensive public transport system largely based on metros, buses and taxis.

In the past 4 decades, the region has experienced an unprecedented rate of rapid and massive urbanization which dramatically altered the landscape and detrimentally affected the ecological conditions in the region. The city's population has increased from 11.04 million at the beginning of the reform and opening-up era in 1978 to 24.25 million in 2014, with the cultivated area decreasing from 3601 to 1990 km^2 during the same time period. In 2014, its gross domestic product (GDP) reached CNY 2.36 trillion (USD 383.55 billion), accounting for 3.7% of the national GDP. The manufacturing, agricultural and service sectors accounted for 34.7, 0.5 and 64.8% of the total output, respectively (Shanghai Municipal Statistics Bureau 2015). The 3 largest service industries are financial services, retail and real estate. Energy consumption increased from 25.53 million tons of coal equivalent (Mtce) in 1985 to 110.84 Mtce in 2014, and CO_2 emissions also increased from 146.50

million tons in 2000 to 420.84 million tons in 2010 (Olivier & Janssens-Maenhout 2011, Shanghai Municipal Statistics Bureau 2015).

2.2. Methodology for CO_2 monitoring

Measurements of atmospheric CO_2 were conducted along 6 transects, with a total length of 335 km, radiating from the central urban core, to cover a range of landscape structure and urbanization gradients (Fig. 1). Of these 6 transects, 3 linear transects followed bearings of northwest (NWT), southwest (SWT) and southeast (SET) and extended for approximately 40 km. The remaining 3 transects were circular transects located on the Inner Ring Road (InnRT, 45 km in length), Middle Ring Road (MidRT, 73 km in length) and Outer Ring Road (OutRT, 97 km in length) in Shanghai.

The Master Urban Plan of Shanghai (1999–2020) (abbreviated as Plan 1999) issued by the Shanghai government clarified officially for the first time that the spatial layout of urbanization in Shanghai is radiated with multi-layers. Therefore, Shanghai's ring roads can be used as layer boundaries to classify the intensity of urbanization, and 2 of the ring roads (Inner Ring Road and Outer Ring Road) are proposed to separate urbanization categories. The Inner Ring Road is the boundary of highly urbanized areas, while areas outside of the Outer Ring Road are considered as suburban and rural areas. Therefore, in our study, we have adopted all 3 ring roads to classify 4 different urbanization gradients: heavy urban (H_urban, within the Inner Ring Road), medium urban (M_urban, outside the Inner Ring Road and within the Middle Ring Road), low urban (L_urban, outside the Middle Ring Road and within the Outer Ring Road) and suburban (S_urban, outside the Outer Ring Road) (Fig.1). The population density and landscape structure obtained based on the decision tree classification (DTC) method (introduced in Section 2.3) are presented in Table 1.

Meteorological conditions and atmospheric stability have a great impact on the concentration of greenhouse gases, especially in urban environments (Aikawa et al. 2006). Intensity of the temperature inversion was moderate in spring (0.93°C per 100 m at 08:00 h) and gradually disappeared after 09:00 h (Yang et al. 2006). Based on the planetary boundary layer (PBL) depths obtained from the NOAA READY archived meteorological GDAS (3 h resolution, 1 × 1°), the PBL depth in Shanghai during spring tended to rise in the morning (~280 m), peak in the mid-afternoon (~750 m) and decrease in the late afternoon (~300 m). According to real-time traffic conditions in Shanghai, the morning rush hour is from 07:00 to 09:00 h, which could give a snapshot of daily air pollution. The sampling time between 09:00 and 11:00 h may be less influenced by automobile exhausts. Therefore, we conducted our

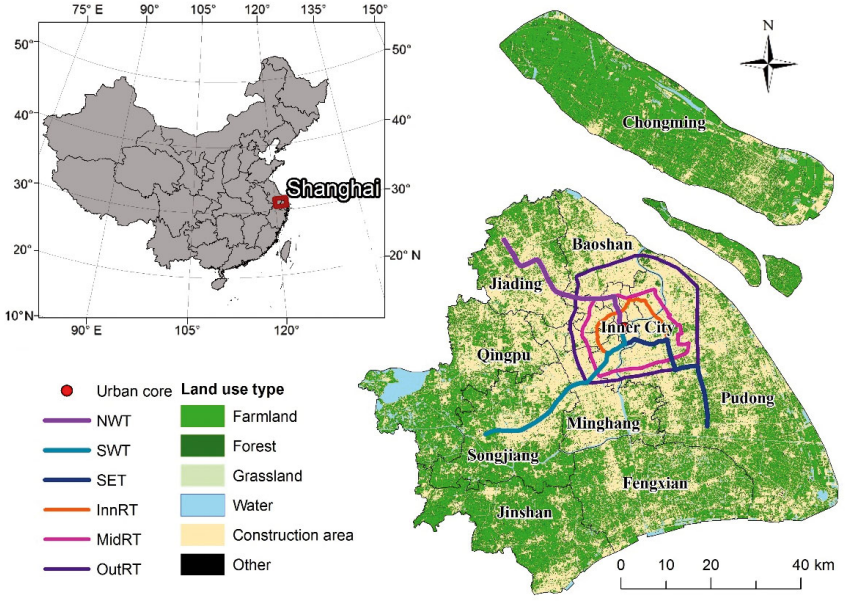

Fig. 1. Land cover in Shanghai, China, and locations of CO_2 measuring routes (thick lines). See Section 2.2 for abbreviations

Table 1. Population and land characteristics for different levels of urbanization in Shanghai. ISA: impervious surface; Veg: vegetation; Wat: water; Oth: other; H_Urban: heavy urban; M_Urban: medium urban; L_Urban: low urban; S_Urban: suburban

	Total area (km^2)	Population density (inhabitants km^{-2})	Landscape structure (%) ISA	Veg	Wat	Oth
H_Urban	113.90	20446	80.44	6.40	11.92	1.24
M_Urban	191.68	8731	78.26	10.04	9.18	2.52
L_Urban	356.72	3403	74.48	14.90	7.15	3.47
S_Urban	2289.80	2883	51.70	38.96	4.71	4.63

in situ measurements during weekday mornings (09:00–11:00 h) on sunny days with clear skies and calm winds from March to April 2014 (Table 2) to ensure better air circulation coupled with relatively low traffic volume. A round trip was made to reduce the uncertainty caused by the discrepancy in time for CO_2 observations. Triplicate measuring trips were made for each transect to obtain a representative and reliable picture of CO_2 within the urban canopy layer. In total, 18 mobile measuring trips were conducted. Beijing (UTC/GMT+08) standard time (BST) is used throughout this study.

CO_2 concentrations were measured by a CO_2/H_2O gas analyzer (LI-840A, LI-COR) and sampled every 10 s at 2 m above ground level, a height in which people are most active. LI-840A is a high-performance, non-dispersive infrared gas analyzer with measurement ranges of 0–20 000 ppm and 0–80 ppt for CO_2 and H_2O, respectively. The accuracies of both detected gases are better than 1.5% of the readings. Bev-A-line tubing (inner diameter: 1/8 inch [3.2 mm]) was used to acquire air intake (2 m in length) and connect the air pump with the analyzer. We used a reference pump (Model 6262-04, LI-COR) for intake of air from the atmosphere and set the velocity of air flow at 1 l min^{-1}. Consequently, the delay time of the LI-840A in this study was 10 s. Driving speed was kept at 35–40 km h^{-1}, with the record interval of the LI-840A set at 10 s during each sampling trip. A GPS (Juno SB, Trimble) was used to acquire location information, with the record interval the same as the analyzer (10 s) during sampling, which provided 2–5 m positional accuracy in real time. With the same record interval, every recorded value of the analyzer was accurately matched to its GPS coordinate. During each sampling campaign, we recorded data for standing time (i.e. traffic lights or traffic jams) along the transects, such as the starting time, location and duration. CO_2 records collected within these standing periods were manually omitted in the data processing. During our sampling, the LI-840A was calibrated before and after each sampling campaign using 2-point calibration. Zero for both CO_2 and H_2O was obtained through inputting dry and pure N_2 (99.9%, Dalian Hede Tech), while the CO_2 span was calibrated through standard gas (490 ppm, National Institute of Metrology, China, which can be traced back to the WMO standard), and the H_2O span was calibrated through an LI-610 portable dew point generator (LI-COR).

2.3. Measurement of urban landscape structure

In this study, the vegetation-impervious surface-soil (V-I-S) model proposed by Ridd (1995) was utilized to describe the landscape structure, which considered the land cover types of the urban environment with high heterogeneity as a linear combination of 3 basic biophysical components, namely vegetation, impervious surface area and bare soil. Due to the low proportion of bare soil in Shanghai, our research focused on vegetation, impervious surface and water area. As there was high cloud coverage with the images around 10 April 2014, 2 cloud-free Landsat 8 Operational Land Imager (OLI) and Thermal Infrared Sensor (TIRS) images (row/path: 038/118 and 039/118), acquired on 29 August 2013, were utilized for the analysis of landscape structure.

In this study, the DTC method (Fayyad & Irani 1992, Chan et al. 2001) was used to divide the complex urban landscape into vegetation (Veg), impervious surface (ISA), water (Wat) and other (Oth) (Fig. 2). We used the normalized difference vegetation index (NDVI), modified normalized difference water index (MNDWI) (Xu 2006) and normalized difference impervious surface index (NDISI) (Xu 2010) to detect the urban complex urban landscape, as follows:

$$NDVI = (NIR - R)/(NIR + R) \quad (1)$$

$$MNDWI = (GREEN - MIR1)/(GREEN + MIR1) \quad (2)$$

$$NDISI = [TIR - (MNDWI + NIR + MIR1)/3]/[TIR + (MNDWI + NIR + MIR1)/3] \quad (3)$$

Table 2. Observation time and meteorological conditions for CO_2 concentrations along 6 transects in Shanghai. NWT: northwest; SWT: southwest; SET: southeast; InnRT: Inner Ring Road; MidRT: Middle Ring Road; OutRT: Outer Ring Road

Transect	Sampling date in 2014 (mo/d)	Weather condition	Wind direction	Wind speed (m s^{-1})
NWT	4/9, 4/11, 4/14	Cloudy, sunny, overcast	NE, SE, E	3.1, 3.6, 3.6
SWT	4/2, 4/4, 4/8	Cloudy, sunny, overcast	E, NW, SE	2.8, 3.6, 5.2
SET	3/26, 3/31, 4/1	Cloudy, sunny, cloudy	E, SE, SE	2.2, 2.8, 3.1
InnRT	4/15, 4/21, 4/22	Sunny, cloudy, sunny	SE, NE, E	2.2, 2.3, 2.2
MidRT	4/23, 4/24, 4/25	Sunny, cloudy, overcast	SE, SE, SE	2.2, 4.0, 5.2
OutRT	4/28, 4/29, 4/30	Cloudy, sunny, sunny	NW, W, S	3.8, 3.1, 2.2

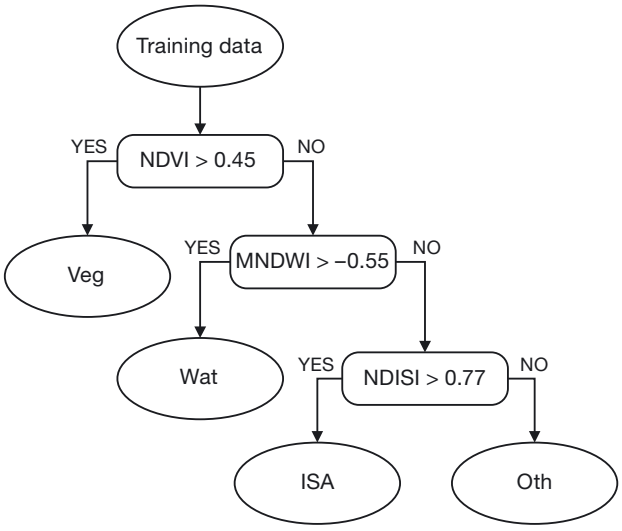

Fig. 2. Procedures of decision tree classification for the extraction of biophysical components of landscape structure including vegetation (Veg), impervious surface (ISA) and water (Wat). NDVI: normalized difference vegetation index; MNDWI: modified normalized difference water index; NDISI: normalized difference impervious surface index; Oth: other

where NIR, R, GREEN, MIR1 and TIR represent the reflectances of near-infrared, red, green, intermediate-infrared and thermal-infrared bands, respectively.

Our classification methodology employs Landsat OLI and TIRS data covering Shanghai to exploit the spectral properties of landscape types. Specifically, we utilized the difference in spatial signatures for impervious surface, vegetation and water area. For example, the signatures for the vegetation and water or impervious plots will vary greatly due to the differences in vegetation abundance during the growing season. The training data included 120 training sites ranging from 900 m^2 (1 pixel) to 90 000 m^2 (10 × 10 pixels) in area, selected and labeled according to manual interpretation of Google Earth imagery (spatial resolution: 4 m; date: 15 April 2014, close to the sampling time). Decision tree constructions involved recursive partitioning of the training data, which were split into increasingly homogeneous subsets based on statistical tests applied to the feature values (Landsat image). Once the decision tree has been estimated and tested to the training data, the decision rules are repeated until all input data have been assigned to one of the target categories (Veg, ISA, Wat and Oth), and a classified map is then produced (Fig. 2).

Additionally, to evaluate the classification accuracy, we randomly selected 100 samples across Shanghai and compared the landscape structure from the DTC method with that obtained from the Google Earth images. The results showed that the overall classification accuracy was 81%, which met the requirements of classification accuracy.

3. RESULTS AND DISCUSSION

3.1. Spatial variation of near-surface CO_2 concentration

The ambient CO_2 concentration between 09:00 and 11:00 h (BST) varied from 370.1 to 588.9 ppm, with an average of 445.8 ± 40.5 ppm. CO_2 concentration exhibited pronounced spatial heterogeneity (Fig. 3), with the highest value in the northwest and the lowest in the southeast. The intensive industrial activities and vehicle fuel combustion are likely significant contributions to elevated CO_2 concentrations. Among the 3 vertical transects (NWT, SET and SWT), CO_2 concentrations were highest in NWT, with an average of 459.9 ± 39.8 ppm. This was partly related to 2 major CO_2 sources (Taopu Industrial Park and Jiading Export Processing Zone) along NWT. SET was lowest in CO_2 concentration, with an average of 429.8 ± 45.0 ppm, and SWT was in-between, with an average of 440.8 ± 31.7 ppm.

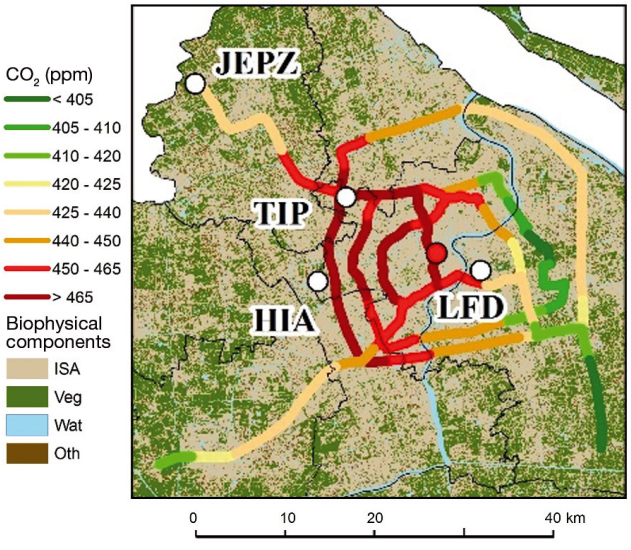

Fig. 3. Spatial distribution of CO_2 concentration along 6 transects in Shanghai. The locations of Taopu Industrial Park (TIP), Jiading Export Processing Zone (JEPZ), Hongqiao International Airport (HIA) and Lujiazui Financial District (LFD) are also shown. ISA: impervious surface; Veg: vegetation; Wat: water; Oth: other

For the 3 circular transects, it is notable that CO_2 concentrations for the westernmost parts of the 3 transects were all above 465 ppm, which was the highest of all 6 transects. This phenomenon might partially be attributed to Hongqiao International Airport (HIA), located west of the 3 ring transects. HIA, with an annual passenger flow of more than 35 million in 2013 (data from Civil Aviation Administration of China), was expected to emit substantial CO_2 because of its intensive flights and concentrated flow of people. However, meteorological conditions also tend to be an important influencing factor for the spatial variation of near-surface CO_2 concentration in Shanghai. The predominantly southeasterly winds during spring might transport a large amount of CO_2 generated in the urban core to the northwestern part of Shanghai and thus elevate the near-surface CO_2 concentration. Near-surface CO_2 concentration in the urban core of Shanghai was, on average, 13.3% higher (55.1 ppm) than that in surrounding areas, which exhibited a well-shaped urban CO_2 dome. This phenomenon was consistent with the findings in Idso et al. (1998) in Phoenix, AZ (Idso et al. 2001). However, the urban CO_2 dome was not representative at a global scale, such as in Essen, Germany (Henninger & Kuttler 2010), and Al-Jahra, Kuwait (Nasrallah et al. 2003), implying that more detailed studies are needed to further understand the mechanism of CO_2 domes in urban areas.

3.2. Variation of CO_2 concentration across urbanization gradients

Based on the classification of urbanization levels in Shanghai, the average atmospheric CO_2 values of H_Urban, M_Urban, L_Urban and S_Urban were 467.6 ± 44.7, 451.7 ± 41.1, 452.7 ± 34.9 and 426.0 ± 24.8 ppm, respectively (Fig. 4). Overall, CO_2 concentration increased with the increase in urbanization levels with the exception that CO_2 in L_Urban was slightly higher than that in M_Urban. This might be attributed to the different traffic volumes in these 2 regions. Since the Pudong part of MidRT was still under construction, its limited traffic volume led to lower CO_2 emissions from automobile exhausts compared to the other 2 ring roads. By contrast, the standard deviations of CO_2 observations strictly decreased with increasing levels of urbanization, suggesting that large uncertainties might exist in monitoring near-surface CO_2 concentration in highly urbanized areas.

With increasing levels of urbanization, the heterogeneity of the underlying surface (Bottema 1997) and

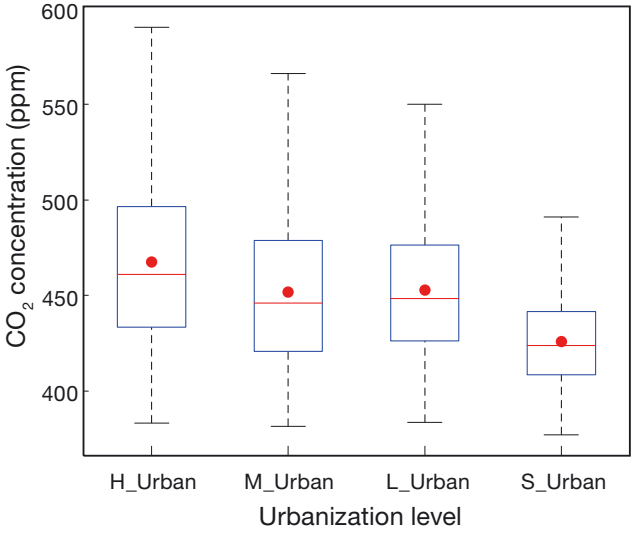

Fig. 4. Box-and-whisker plots of CO_2 concentration for different urbanization levels during the study period. Red dots: mean value of CO_2 concentration for each urbanization level; red lines: median of CO_2 concentrations for each urbanization level; top and bottom of boxes: upper and lower quartiles of CO_2 concentrations for each urbanization level; top and bottom of the whiskers: maximum and minimum CO_2 concentrations for each urbanization level. H_Urban: heavy urban; M_Urban: middle urban; L_Urban: low urban; S_Urban: suburban

the roughness of the city (Rotach 1999), such as urban construction (Ng et al. 2011), have increasingly complex influences on local meteorological conditions (such as reduced wind speed and no sustained wind direction) accompanied by an increase in the spatial heterogeneity of carbon emissions (Bergeron & Strachan 2011, Crawford et al. 2011). Therefore, near-surface CO_2 concentration will be affected by the interactions of more complex controlling factors. Notably, the median CO_2 concentration calculated for a certain urbanization level was always below the mean CO_2 concentration, irrespective of any urbanization level (see Fig. 4). Likewise, the distance between the maximum and upper quartile surpassed the distance between the minimum and lower quartile. Both indicated that deviations were mainly from short periods of higher values, which was the major shortcoming of mobile measurements (Wentz et al. 2002). To overcome this, further studies need to take greater account of the so-called distance–decay effect to get more accurate values, since the concentration we get may be higher than the undisturbed conditions.

Rapid urban sprawl and the increase in urbanization have a significant impact on carbon emissions and cycling (Imhoff et al. 2004, George et al. 2007). We

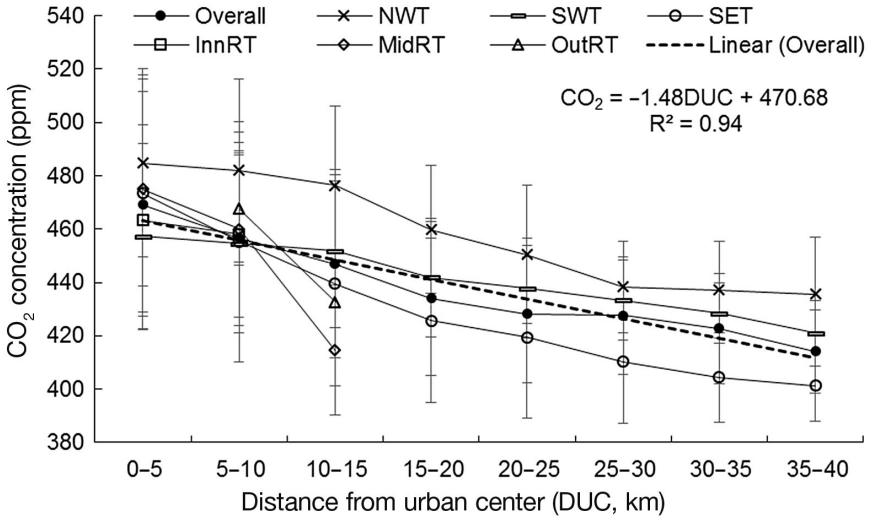

Fig. 5. Relationship between distance from the urban core (DUC) and near-surface CO_2 concentration. Error bars: standard deviation of CO_2 concentration. The formula in the upper right corner shows the linear fitting curve of the overall samples from 6 transects. NWT: northwest; SWT: southwest; SET: southeast; InnRT: Inner Ring Road; MidRT: Middle Ring Road; OutRT: Outer Ring Road

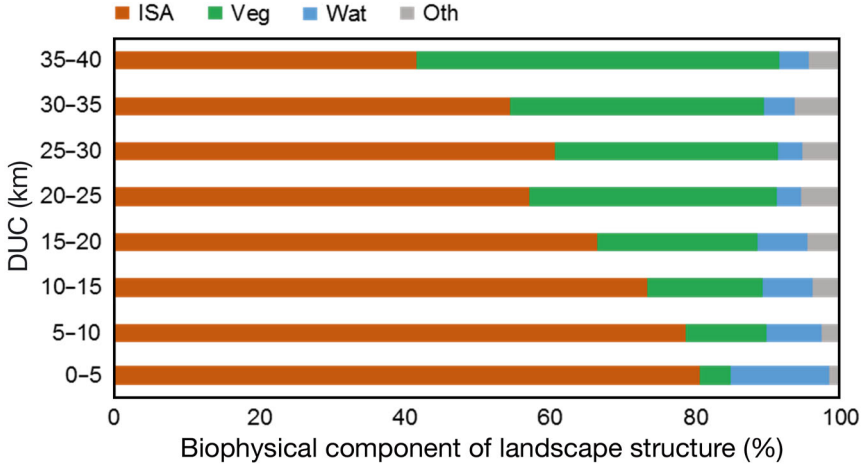

Fig. 6. Variation of biophysical components of landscape structure with different distances from the urban core (DUC). ISA: impervious surface; Veg: vegetation; Wat: water; Oth: other

presented a linear function to simulate the relationship between CO_2 concentration and distance from the urban core (DUC). A significant decrease in CO_2 concentration was observed as DUC increased (CO_2 = −1.48DUC + 470.68, R^2 = 0.94, $p < 0.01$, Fig. 5). The 3 vertical transects showed significant urban–suburban differences; differences were the biggest in SET (72.1 ppm), in-between in NWT (49.2 ppm) and the smallest in SWT (36.3 ppm). Overall, CO_2 concentration had the biggest decline over 15–20 km DUC (approximately 12.9 ppm) and the smallest decline over 20–25 km DUC (less than 1 ppm), which indicated that a DUC of 20 km tends to be a threshold for the decline in CO_2 concentration in Shanghai. Within the range of 20 km DUC, CO_2 concentration declined significantly (approximately 1.8 ppm km^{-1}), while outside of 20 km DUC, CO_2 concentration declined much more slowly (approximately 0.7 ppm km^{-1}). Coincidentally, 20 km DUC is where OutRT is situated, and according to Plan 1999, OutRT was regarded as the boundary separating urban areas from suburban and rural areas. Hence, differences in urbanization level within OutRT were more marked, causing a larger decline in CO_2 concentration, while areas outside of OutRT tended to be less affected by urbanization level, with smaller declining rates.

3.3. Relationship between CO_2 concentration and landscape structure

According to the spatial pattern of landscape structure based on the DTC method, ISA decreased and Veg increased significantly with the increase of DUC (Fig. 6). Among the 3 biophysical components, Veg varied the most, from 4.37% at 0–5 km to 49.87% at 35–40 km. ISA decreased its proportion by almost half. The proportion for Wat was always below 10%, with little change except at a DUC of 0–5 km (close to the Huangpu River). At around a DUC of 25–30 km ISA increased a little and Veg had a homologous decrease, which was opposite to the overall trend. As mentioned in Section 3.2, a DUC of 20 km was close to where OutRT is situated.

To further explore the relationship between spatial patterns of CO_2 concentration and biophysical components of landscape structure, we divided all 6 transects into 335 parts (1 km each). The Pearson correlation coefficient (R) between CO_2 concentration and each biophysical component was calculated within a certain spatial scale of different buffer distances. The results indicated that near-surface CO_2 concentration was significantly correlated with ISA and Veg ($p <$

Table 3. Pearson's correlation relationship between CO_2 concentration and impervious surface (ISA), vegetation (Veg) and water (Wat) with buffer distances from 1 to 7 km. Significance: $^{*}p < 0.05$, $^{**}p < 0.01$

Buffer distance (km)	CO_2 and ISA	CO_2 and Veg	CO_2 and Wat
1	0.43**	−0.044**	0.16**
2	0.52**	−0.52**	0.16*
3	0.56**	−0.56**	0.12*
4	0.62**	−0.61**	0.10
5	0.67**	−0.63**	0.04
6	0.61**	−0.60**	0.06
7	0.58**	−0.56**	0.04

0.01) (Table 3). These results are similar to those in Montreal, Canada (Bergeron & Strachan 2011), where CO_2 emission for urban (ISA and Veg: 71 and 29%, respectively) and suburban sites (ISA and Veg: 49 and 50%, respectively) were 20.6 and 5.4 kg CO_2 m^{-2} a^{-1} higher, respectively, than the background value (−0.2 kg CO_2 m^{-2} a^{-1}) for agriculture (0 and 100%, respectively).

Since atmospheric CO_2 concentration could merely represent the results of interactions of biophysical components at a certain spatial scale, we evaluated the R value between CO_2 concentration and ISA or Veg when the buffer distance varied from 1 to 7 km. The results showed that the correlation between CO_2 concentration and both ISA and Veg increased first and then decreased with the increase in buffer distance (ISA: R = 0.43–0.67; Veg: R = −0.44 to −0.63), and they both achieved their highest value when the buffer distance was 5 km. Thus, a certain spatial scale with a buffer distance of 5 km was used to examine how the biophysical components exercised an influence on CO_2 concentration.

On this basis, a series of multiple regression models, i.e. linear, exponential, logarithmic and power function, were developed to simulate the relationship between CO_2 concentration and ISA or Veg with a buffer distance of 5 km. The results showed that the linear function worked better than the other models (Fig. 7). The linear fitting equation was obtained through a stepwise regression analysis, with CO_2 concentration as the dependent variable and both ISA and Veg as the independent variables:

$$CO_2 = 0.99ISA - 0.18Veg + 378.18 \quad (R^2 = 0.44, p < 0.01) \quad (4)$$

We can conclude from the regression equation that CO_2 concentration increases 0.99 ppm for every 1% that ISA increases, and decreases 0.18 ppm for every 1% that Veg increases, which means the influence of ISA on CO_2 concentration was significantly higher than the influence of Veg. The underlying cause for this difference is that the amount of CO_2 emissions in urban areas was much high than the CO_2 sequestration caused by urban vegetation (Nordbo et al. 2012, Hutyra et al. 2014), although urban vegetation acts as a sink for fossil fuel emissions and thereby slows the rise of atmospheric CO_2 concentration. The trend in atmospheric CO_2 in urban areas was likely to depend more on fossil fuel emissions than on vegetation change. This conclusion was similar to the results acquired from a meta-analysis based on 14 annual CO_2 budget studies and an extraction of 56 individual cities that corroborates the study's inventory-based estimates (Nordbo et al. 2012), which pointed out that the fraction of natural area was the strongest predic-

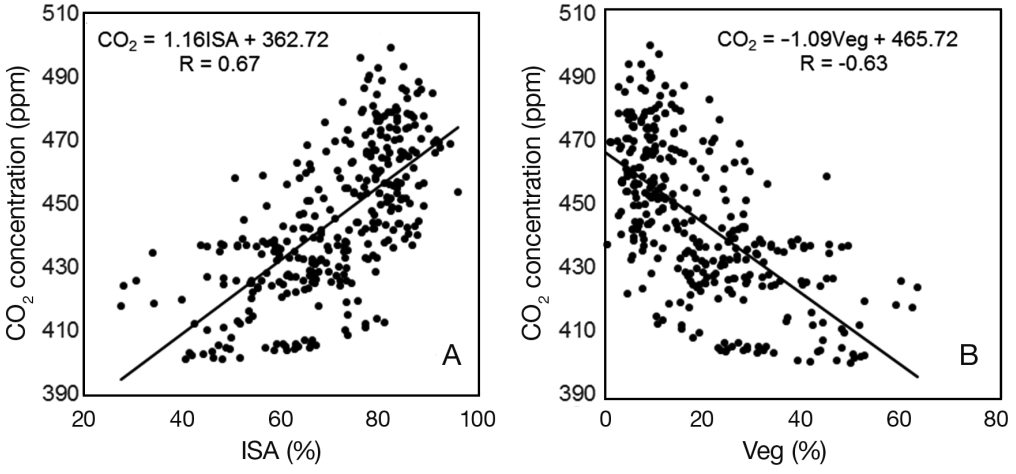

Fig. 7. Linear relationship between CO_2 concentration and (A) impervious surface (ISA) or (B) vegetation (Veg) when buffer distance was 5 km

tor of urban CO_2 budgets. Cities were considered as a carbon source once the urban fraction was over 20% (urban fraction = 1 − natural fraction). In a simulation of the spatial distribution of CO_2 concentration in Shenyang, China, Wang & Wei (2012) also concluded that the top third of CO_2 concentration was generated by 3 land use types: transportation land, high-density construction and low-density construction. In addition, at the observation station in the Cub Hill suburb of Baltimore, MD, the small amount of ISA (31.4%) and abundant Veg (67.4%) (Crawford et al. 2011) were not enough to offset local emissions by anthropogenic activity. The CO_2 flux in a low-storied residential area (May 2010–April 2011) in Tokyo, Japan (Moriwaki & Kanda 2004), was 6 times the downward CO_2 flux at a typical temperate deciduous forest, which could also verify the important influence of ISA on CO_2 concentration to a certain extent.

4. CONCLUSIONS

Mobile measurements of urban daytime CO_2 from 6 transects totaling 335 km in length were conducted in Shanghai, the commercial and financial center of China. These high spatial resolution CO_2 measurements provided the opportunity to understand the spatial patterns of urban atmospheric CO_2 concentration and to investigate its relationship with the underlying surface, i.e. the landscape structure across urbanization gradients. The average daytime ambient CO_2 concentration along these 6 transects in Shanghai was 445.8 ± 40.5 ppm from March to April 2014, while average CO_2 concentration in the urban core was 13.3% higher (55.1 ppm) than that in surrounding areas, which exhibited a well-shaped urban CO_2 dome. Also, CO_2 concentration in Shanghai showed a significant spatial variability, with the highest concentration appearing in the northwest followed by the southwest and the lowest concentration appearing in the southeast, in accordance with the urbanization gradients of the underlying surface. The results indicated that there was a significant relationship between ambient CO_2 concentration and the underlying surface. The percent of impervious surface cover was an important indicator of atmospheric CO_2 concentration, with a positive correlation, while the vegetation area had a negative correlation, but with a lower explanatory power. This result implied that the trend in atmospheric CO_2 in urban areas was likely to depend more on fossil fuel emissions than on vegetation change. When the buffer distance was 5 km, the correlation coefficient between CO_2 concentration and urban landscape structure achieved its highest value. Their quantitative relationship could be described by the stepwise regression equation $CO_2 = 0.99ISA - 0.18Veg + 378.18$ ($R^2 = 0.44$, $p < 0.01$).

Our work focused on the relationship between the CO_2 concentration and the land fraction. The CO_2 measurements are assumed to be representative at the regional level, resulting in high uncertainties in estimation of regional CO_2 concentration. However, direct validation of regional-scale CO_2 with high spatial resolution is not possible due to the great difficulty in conducting CO_2 observations covering the whole city. Nevertheless, the high correspondence of our city-scale estimates supports the robustness of the new method. Additional studies on urban CO_2 concentrations in different parts of the world, with longer measuring periods and different measurement heights are also needed to represent diverse urban forms (higher or lower urban fraction) and climates (Asia, Africa and America).

Acknowledgements. This study was supported by the National Natural Science Foundation of China (41201092 and 41471076) and Shanghai Pujiang Program (14PJ 1402800). The authors thank Xiaoyan Zhao for technical assistance with the LI-840A. We are also very grateful to 3 anonymous reviewers for providing invaluable suggestions and comments, which helped us to improve this manuscript.

LITERATURE CITED

Aikawa M, Hiraki T, Eiho J (2006) Vertical atmospheric structure estimated by heat island intensity and temporal variations of methane concentrations in ambient air in an urban area in Japan. Atmos Environ 40:4308–4315

Bergeron O, Strachan IB (2011) CO_2 sources and sinks in urban and suburban areas of a northern mid-latitude city. Atmos Environ 45:1564–1573

Bottema M (1997) Urban roughness modelling in relation to pollutant dispersion. Atmos Environ 31:3059–3075

Büns C, Kuttler W (2012) Path-integrated measurements of carbon dioxide in the urban canopy layer. Atmos Environ 46:237–247

Chan JCW, Chan KP, Yeh AGO (2001) Detecting the nature of change in an urban environment: a comparison of machine learning algorithms. Photogramm Eng Remote Sensing 67:213–225

Churkina G (2008) Modeling the carbon cycle of urban systems. Ecol Modell 216:107–113

Crawford B, Grimmond CSB, Christen A (2011) Five years of carbon dioxide fluxes measurements in a highly vegetated suburban area. Atmos Environ 45:896–905

Energy Information Administration (2013) International Energy Outlook 2013. DOE/EIA-0484, Energy Information Administration, Office of Energy Analysis, US Dep Energy, Washington, DC

Fang SX, Zhou LX, Tans PP, Ciais P, Steinbacher M, Xu L, Luan T (2014) In situ measurement of atmospheric CO_2

at the four WMO/GAW stations in China. Atmos Chem Phys 14:2541–2554

Fayyad UM, Irani KB (1992) On the handling of continuous-valued attributes in decision tree generation. Mach Learn 8:87–102

George K, Ziska LH, Bunce JA, Quebedeaux B (2007) Elevated atmospheric CO_2 concentration and temperature across an urban–rural transect. Atmos Environ 41: 7654–7665

Grimmond C, Christen A (2012) Flux measurements in urban ecosystems. FluxLetter–Newsetter of Fluxnet 5:1–7

Grimmond CS, King TS, Cropley FD, Nowak DJ, Souch C (2002) Local-scale fluxes of carbon dioxide in urban environments: methodological challenges and results from Chicago. Environ Pollut 116, Suppl 1:S243–S254

Henninger S (2008) Analysis of near surface CO_2 variability within the urban area of Essen, Germany. Meteorol Z 17: 19–27

Henninger S, Kuttler W (2010) Near surface carbon dioxide within the urban area of Essen, Germany. Phys Chem Earth 35:76–84

Hutyra LR, Duren R, Gurney KR, Grimm N, Kort EA, Larson E, Shrestha G (2014) Urbanization and the carbon cycle: current capabilities and research outlook from the natural sciences perspective. Earths Futur 2:473–495

Idso CD, Idso SB, Balling RC Jr (1998) The urban CO_2 dome of Phoenix, Arizona. Phys Geogr 19:95–108

Idso CD, Idso SB, Balling RC Jr (2001) An intensive two-week study of an urban CO_2 dome in Phoenix, Arizona, USA. Atmos Environ 35:995–1000

Imhoff ML, Bounoua L, DeFries R, Lawrence WT, Stutzer D, Tucker CJ, Ricketts T (2004) The consequences of urban land transformation on net primary productivity in the United States. Remote Sens Environ 89:434–443

IPCC (2013) Climate change 2013: the physical science basis. In: Stocker TF, Qin D, Plattner GK, Tignor M and others (eds) Contribution of Working Group I to the Fifth Assessment Report of the Intergovernmental Panel on Climate Change. Cambridge University Press, New York, NY

Keeling CD, Bacastow RB, Bainbridge AE, Ekdahl CA, Guenther PR, Waterman LS, Chin JFS (1976) Atmospheric carbon dioxide variations at Mauna Loa Observatory, Hawaii. Tellus 28:538–551

Kort EA, Frankenberg C, Miller CE, Oda T (2012) Space-based observations of megacity carbon dioxide. Geophys Res Lett 39:L17806, doi:10.1029/2012GL052738

Le Quéré C, Raupach MR, Canadell JG, Marland G and others (2009) Trends in the sources and sinks of carbon dioxide. Nat Geosci 2:831–836

Liu M, Wu J, Zhu X, He H, Jia W, Xiang W (2015) Evolution and variation of atmospheric carbon dioxide concentration over terrestrial ecosystems as derived from eddy covariance measurements. Atmos Environ 114:75–82

Makido Y, Dhakal S, Yamagata Y (2012) Relationship between urban form and CO_2 emissions: evidence from fifty Japanese cities. Urban Clim 2:55–67

Moriwaki R, Kanda M (2004) Seasonal and diurnal fluxes of radiation, heat, water vapor, and carbon dioxide over a suburban area. J Appl Meteorol 43:1700–1710

Nasrallah HA, Balling Jr RC, Mohammed Madi S, Al-Ansari L (2003) Temporal variations in atmospheric CO_2 concentrations in Kuwait City, Kuwait with comparisons to Phoenix, Arizona, USA. Environ Pollut 121:301–305

Ng E, Yuan C, Chen L, Ren C, Fung JCH (2011) Improving the wind environment in high-density cities by understanding urban morphology and surface roughness: a study in Hong Kong. Landsc Urban Plan 101:59–74

Nordbo A, Järvi L, Haapanala S, Wood CR, Vesala T (2012) Fraction of natural area as main predictor of net CO_2 emissions from cities. Geophys Res Lett 39:L20802, doi: 10.1029/2012GL053087

Olivier J, Janssens-Maenhout G (2011) III. Greenhouse gas emissions. In: CO_2 emissions from fuel combustion. JRC 67519, International Energy Agency, Paris, p III.1–III.57

Ou J, Liu X, Li X, Chen Y (2013) Quantifying the relationship between urban forms and carbon emissions using panel data analysis. Landsc Ecol 28:1889–1907

Ridd MK (1995) Exploring a V-I-S (vegetation-impervious surface-soil) model for urban ecosystem analysis through remote sensing: comparative anatomy for cities. Int J Remote Sens 16:2165–2185

Rotach MW (1999) On the influence of the urban roughness sublayer on turbulence and dispersion. Atmos Environ 33:4001–4008

Sasakawa M, Machida T, Tsuda N, Arshinov M, Davydov D, Fofonov A, Krasnov O (2013) Aircraft and tower measurements of CO_2 concentration in the planetary boundary layer and the lower free troposphere over southern taiga in West Siberia: long-term records from 2002 to 2011. J Geophys Res 118:9489–9498

Shanghai Municipal Statistics Bureau (2015) Shanghai statistical yearbook 2014. China Statistics Press, Beijing

Stephens BB, Brailsford GW, Gomez AJ, Riedel K, Mikaloff Fletcher SE, Nichol S, Manning M (2013) Analysis of a 39-year continuous atmospheric CO_2 record from Baring Head, New Zealand. Biogeosciences 10:2683–2697

Stocker BD, Roth R, Joos F, Spahni R and others (2013) Multiple greenhouse-gas feedbacks from the land biosphere under future climate change scenarios. Nat Clim Change 3:666–672

Velasco E, Roth M (2010) Cities as net sources of CO_2: review of atmospheric CO_2 exchange in urban environments measured by eddy covariance technique. Geogr Compass 4:1238–1259

Wang L, Wei Y (2012) Simulation of spatial distribution of carbon emissions in Shenyang City based on remote sensing and GIS. Resour Sci 34:328–336 (in Chinese)

Wentz EA, Gober P, Balling RC Jr, Day TA (2002) Spatial patterns and determinants of winter atmospheric carbon dioxide concentrations in an urban environment. Ann Assoc Am Geogr 92:15–28

WMO (2012) Greenhouse gas bulletin: the state of greenhouse gases in the atmosphere based on global observations through 2011. WMO, Geneva

Wu J, Guan D, Yuan F, Yang H, Wang A, Jin C (2012) Evolution of atmospheric carbon dioxide concentration at different temporal scales recorded in a tall forest. Atmos Environ 61:9–14

Xu H (2006) Modification of normalised difference water index (NDWI) to enhance open water features in remotely sensed imagery. Int J Remote Sens 27:3025–3033

Xu H (2010) Analysis of impervious surface and its impact on urban heat environment using the normalized difference impervious surface index (NDISI). Photogramm Eng Remote Sensing 76:557–565

Yang Y, Tan J, Zheng Y, Cheng S (2006) Study on the atmospheric stabilities and the thickness of atmospheric mixed layer during recent 15 years in Shanghai. Sci Meteorol Sin 26:536–541 (in Chinese)

Zhang D, Tang J, Shi G, Nakazawa T and others (2008) Temporal and spatial variations of the atmospheric CO_2 concentration in China. Geophys Res Lett 35:L03801, doi: 10.1029/2008GL033222

Editorial responsibility: Eduardo Zorita, Geesthacht, Germany

Submitted: August 17, 2015; Accepted: April 5, 2016
Proofs received from author(s): June 2, 2016